Inorganic Chemistry

Article

pubs.acs.org/IC

Microporous Hexanuclear Ln(III) Cluster-Based Metal–Organic Frameworks: Color Tunability for Barcode Application and Selective Removal of Methylene Blue

Ming-Liang Gao,[†] Wen-Jing Wang,[‡] Lin Liu,[†] Zheng-Bo Han,*[,†] Na Wei,[†] Xiao-Man Cao,[†] and Da-Qiang Yuan*[,‡]

[†]College of Chemistry, Liaoning University, Shenyang 110036, P. R. China

[‡]State Key Laboratory of Structural Chemistry, Fujian Institute of Research on the Structure of Matter, Chinese Academy of Sciences, Fuzhou 350002, P. R. China

Supporting Information

ABSTRACT: Two hexanuclear Ln(III) cluster-based metal–organic frameworks (MOFs) (Ln = Tb or Eu) and a series of isomorphic bimetallic Ln(III)-MOFs have been synthesized by changing the ratio of Tb(III) and Eu(III) under solvothermal conditions. The excellent linear color tunability (from green to red) makes them suitable for barcode application. In addition, the anionic Ln(III)-MOFs exhibit superior uptake capacity toward methylene blue (MB^+) by an ion-exchange process, and its reversible adsorption performance makes **1** suitable for removal of organic dye MB^+. The as-prepared anionic hexanuclear Ln(III) cluster-based MOFs can serve as a multifunctional material for an optical and environmental area.

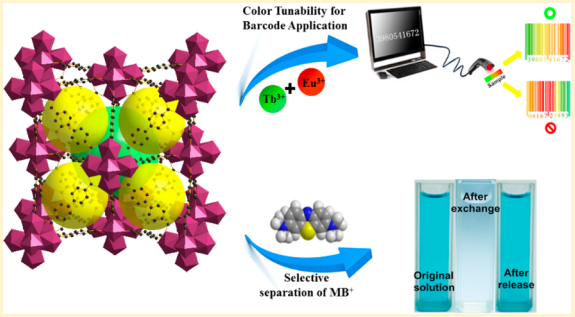

INTRODUCTION

Barcoded material[1] on labels has been a considerable focus for multiplexed bioanalytical science and antiforgery application (Scheme 1).[2] A perfect barcoded material should meet some requirements. The material ought to be robust and securable on large scale;[3] its synthetic strategy should be straightforward and highly repeatable, and its spectral absorption or emission signal should be easily detected and unambiguously rendered.[4] In addition, it is necessary to provide plentifully feasible coding combinations.[5] Today, multiband barcoded materials have been principally prepared with organic luminescence dyes[6] or semiconductor quantum dots,[7] which were implanted into organic conjugated polymers or inorganic silica colloids. Nevertheless, organic fluorescein has broad emission bands, which lead to the spectroscopic overlap, and a portion of the securable characteristic bands for barcoded materials can also be limited. Although quantum dot materials could emit a relatively narrow spectroscopy characteristic signal, they were universally prepared with toxic substances (e.g., CdSe, CdS, and CdTe).[8] In recent years, developing novel lanthanide [Ln(III)]-based luminescent material with controlled and fine-tuned property for barcode material has been a very active field. Ln(III)-based luminescent barcode materials have unparalleled peculiarities in comparison with the organic fluorescein and semiconductor quantum dots, including narrow emission characteristic bands, nonoverlapping spectra, large Stokes shifts, and high color purity.[9] Most importantly, every Ln(III) cation has its characteristic emission peaks, which could not be affected by their environment. This feature means Ln(III) luminescence barcodes can be used in various materials and solvents. On the other hand, organic chromophore ligands always can be used to sensitize the free Ln(III) because of its very low extinction coefficient. To achieve efficient sensitization, it is very important to place the chromophore ligands and Ln(III) at the proper location for energy transfer.

Scheme 1. Demonstration of Using the Present Materials for Encryption Strips and Anticounterfeiting Technology with Numerous Possible Encoding Combinations

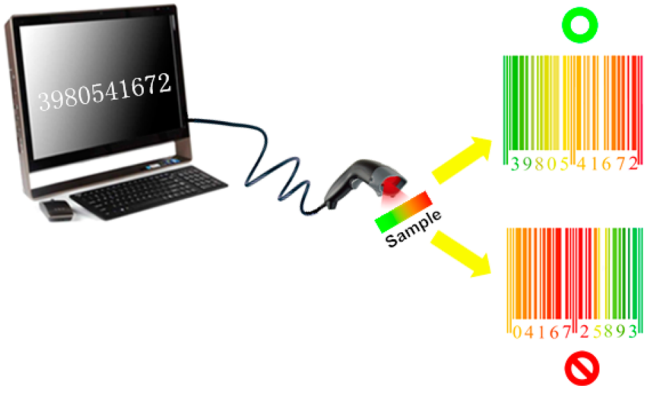

Received: October 4, 2016
Published: December 12, 2016

DOI: 10.1021/acs.inorgchem.6b02413
Inorg. Chem. 2017, 56, 511–517

Recent research has shown that Ln(III) metal−organic frameworks [Ln(III)-MOFs] are very promising platforms because the Ln(III) ions and sensitizers can be organized into long-range ordered structure to allow dense packing and enhanced emission while minimizing self-quenching.[10] In addition, by using a single excitation wavelength, different Ln(III) cations can be sensitized at the same time by judicious selection of the chromophoric ligands to realize the concurrent emission of multiple bands, which could satisfy the applicable requirements of barcode materials. The first barcode system based on mixed metallic Ln(III)-MOFs was prepared by Rosi and Petoud. In this study, bimetallic near-infrared (near-IR) Ln(III)-MOFs that emit near-IR optical signals were linearly correlated to the mixed Ln(III) ion ratio.[5] However, the high-nuclearity Ln(III) cluster-based MOFs used for barcoded materials are still rare. If we choose proper cations, such as Tb^{3+} and Eu^{3+}, the prepared bimetallic MOFs might exhibit a higher energy transfer efficiency between different Ln(III) ions because of the dense packing of Ln(III) ions in high-nuclearity cluster MOFs. With this in mind, we synthesized microporous hexanuclear Ln(III) cluster-based MOFs **1** (Tb) and **2** (Eu) by a solvothermal method. By accurately controlling the mixed Ln(III) cationic content in Ln(III)-MOFs, we achieved dichromatic fine adjustment among red or green primary colors by generating a series of isomorphous Ln(III)-MOF **3**−**6**. In addition, **1** is an anionic framework, which shows excellent adsorption capacity for methylene blue (MB^+) through an ion-exchange process.

EXPERIMENTAL SECTION

Materials and General Procedures. All starting ligands (H_2BPDC and 2-fluorobenzoic acid), $Ln(NO_3)_3{\cdot}6H_2O$ (99.99%), and solvents employed in this work were used without further purification. Elemental analyses (EA) of C, H, and N were performed with a PerkinElmer 240 analyzer. The Fourier transform infrared (FT-IR) spectra using KBr pellets were recorded on a Nicolet 5DX spectrometer in the of range 4000−400 cm^{-1}. Powder X-ray diffraction (PXRD) spectra were recorded on a Bruker AXS D8 advanced automated diffractometer at 40 kV and 40 mA with Cu Kα radiation. Thermogravimetric (TG) analyses were performed on a PerkinElmer Pyrisl analyzer [298−1176 K, heating rate of 5 K min^{-1}, flowing N_2 (g)]. Inductively coupled plasma-optical emission spectroscopy (ICP-OES) data were collected on an Agilent Technologies 700 Series ICP-OES instrument. Luminescence spectroscopy and lifetime data for the solid samples were collected on a FLSP920 Edinburgh fluorescence spectrometer at room temperature. All the UV/vis absorption data were collected using a SP-752(PC) UV−vis spectrophotometer.

Synthesis of $(DMA)_2[Tb_6(\mu_3\text{-}OH)_8(BPDC)_6]{\cdot}x$(Solvent) (1). $Tb(NO_3)_3{\cdot}6H_2O$ (9 mg, 0.0225 mmol), H_2BPDC (5 mg, 0.0225 mmol), and 2-fluorobenzoic acid (95.2 mg, 0.675 mmol) were added to a 20 mL scintillation vial with a mixed solvent of DMF (2 mL) and EtOH (0.5 mL) and stirred for 0.5 h at room temperature. Then the mixture was preserved at 378 K for 36 h and slowly cooled (cooling rate of 5 K h^{-1}) to room temperature to obtain the polyhedral crystals of **1**. The as-prepared crystals were washed with DMF and air-dried at room temperature (yield of ∼53%). In addition, DMF solvent decomposed at 378 K to form countercation DMA^+ (dimethylamine cation). EA. Calcd (%) for **1**, $C_{88}H_{72}Tb_6O_{32}N_2$ (%): C, 40.29; H, 2.77; N, 1.07. Found: C, 40.23; H, 2.67; N, 1.03. FT-IR (KBr pellets): 3425 (s), 2931 (w) 1666 (vs), 1605 (s), 1542 (m), 1404 (vs), 1250 (m), 1172 (m), 1095 (m), 846 (m), 771 (m), 663 (w), 555 (m) cm^{-1}.

Synthesis of $(DMA)_2[Eu_6(\mu_3\text{-}OH)_8(BPDC)_6]{\cdot}x$(Solvent) (2). **2** was obtained by a procedure similar to that used for **1** except for using $Eu(NO_3)_3{\cdot}6H_2O$ instead of terbium nitrate. Yield: 66%. EA. Calcd for $C_{88}H_{72}Eu_6O_{32}N_2$: C, 40.95; H, 2.81; N, 1.09. Found: C, 39.56; H, 2.31; N, 1.12. FT-IR (KBr pellets): 3426 (s), 2930 (w), 1668 (vs), 1604 (s), 1542 (m), 1405 (vs), 1252 (m), 1172 (m), 1094 (m), 844 (m), 772 (m), 664 (w), 553 (m) cm^{-1}.

X-ray Crystallography. Single-crystal diffraction data of complexes **1** and **2** were collected at 100 K with a Bruker AXS smart Apex CCD II diffractometer using Mo Kα (λ = 0.71073 Å) radiation and a SuperNova, Dual, Cu at zero, Atlas diffractometer with Cu Kα (λ = 1.5418 Å) radiation, respectively. The structure was determined by direct methods using SHELXS-97 and refined on F^2 by full-matrix least squares with the SHELXTL-97 crystallographic software package.[11] DMA^+ cations and guests were highly disordered. The diffused electron densities resulting from these residual molecules were removed from the data set using the SQUEEZE[12] routine of PLATON and refined further using the data generated. Crystallographic data and experimental details for structural analyses are summarized in Table S1. The CCDC reference numbers were 1454038 and 1454039 for **1** and **2**, respectively. A copy of the data can be obtained free of charge on application to CCDC, 12 Union Road, Cambridge CB2 1EZ, U.K. [fax: int code +44(1223)336-033; e-mail: deposit@ccdc.cam.ac.uk].

Synthesis of $(DMA)_2[Eu_{6x}Tb_{6(1-x)}(\mu_3\text{-}OH)_8(BPDC)_6]{\cdot}x$(Solvent) (3−6). **3**−**6** were synthesized using a procedure similar to that used for **1** in which mixed $Eu(NO_3)_3{\cdot}6H_2O$ (0.0225x mmol) and $Tb(NO_3)_3{\cdot}6H_2O$ [0.0225(1 − x) mmol] [x = 0.0005 (**3**), 0.0010 (**4**), 0.0050 (**5**), and 0.0075 (**6**)] were substituted for $Tb(NO_3)_3{\cdot}6H_2O$. The obtained colorless polyhedral crystals were washed with DMF and air-dried at room temperature.

Selective Removal and Separation of an Organic Dye. The prepared **1** (20 mg) was soaked in 5 mL DMF solutions in which different organic dyes were dissolved (5×10^{-5} M) and monitored by UV−vis spectra at room temperature. The desorption experiment with MB^+@**1** was performed after the cation-exchange process of MB^+ on anionic **1**. Then, MB^+@**1** was successively soaked in the pure DMF solution (5 mL) and a saturated NaCl/DMF solution (5 mL).

RESULTS AND DISCUSSION

Crystal Structure. Single-crystal XRD data analysis demonstrates that **1** and **2** are isomorphic, so only complex **1** is described here in detail. As shown Figure 1, this crystallizes in cubic space group $Fm\bar{3}m$. Each Tb^{3+} was encircled by four μ_3-OH groups, four oxygen atoms from the carboxylate groups of independent BPDC ligands (Figure 1a).[13] Six adjacent Tb^{3+} cations were linked by eight μ_3-OH groups to form a

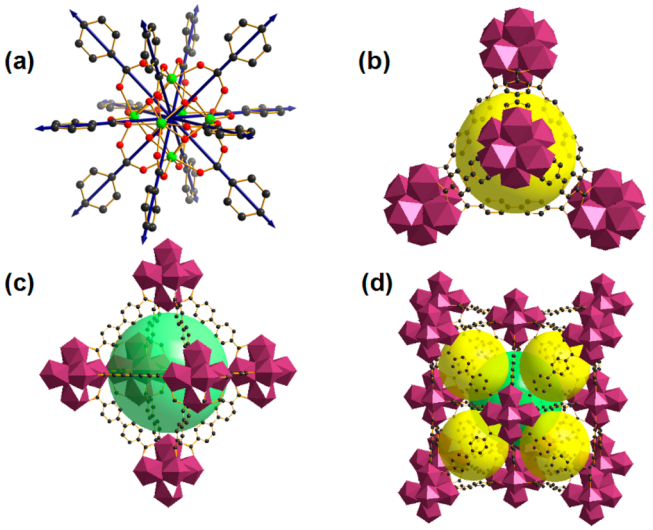

Figure 1. (a) Ball-and-stick representation of the BPDC ligand and hexanuclear unit, $[Tb_6(\mu_3\text{-}OH)_8(COO)_{12}]$ (black for C, red for O, and green for Tb). (b) Tetrahedral cage. (c) Octahedral cage. (d) In **1**, packing of two types of cages.

DOI: 10.1021/acs.inorgchem.6b02413
Inorg. Chem. 2017, 56, 511−517

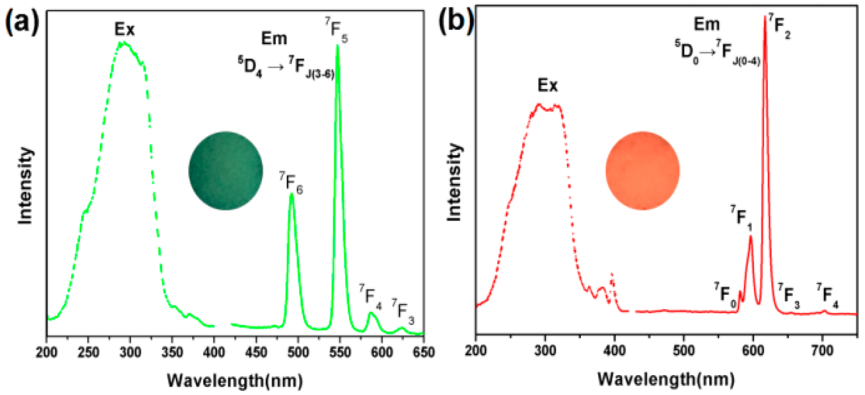

Figure 2. (a) Excitation and emission spectra of **1**. (b) Excitation and emission spectra of **2**.

hexanuclear unit. Each hexanuclear unit was linked by 12 BPDC ligands to construct a 12-connected three-dimensional MOF. Two types of microporous polyhedral cages, the tetrahedral cages with an estimated diameter of 1.2 nm and the octahedral cages with an estimated diameter of 1.6 nm, were constructed by the self-assembly of the hexanuclear units and bridging ligands (Figure 1b–d). The theoretical void ratio of **1** is 70%, calculated with PLATON.[14]

Thermal Stability. TG analysis showed that all lattice molecules could be evacuated upon heating of the sample to 160 °C (Figure S1). The phase purity of the hexanuclear Ln(III) cluster-based MOFs was confirmed by PXRD (Figure S2). Additionally, the hexanuclear Ln(III) cluster-based MOF exhibits favorable chemical stability (Figure S3), which is a crucial factor for developing its relevant applications.

Luminescence Properties of the Hexanuclear Ln(III) Cluster-Based MOF. Luminescent Ln(III)-based MOF materials usually emit sharp characteristic bands with different colors. For this reason, designing luminescent Ln(III)-based MOFs is an advisable choice for acquiring tunable optical materials.[4,15] To obtain good optical materials, we investigated the luminescence properties of **1** and **2**. The excitation and emission spectra of **1**, **2**, and H_2L are shown in Figure 2 and Figure S4. The luminescence emission spectra of power samples **1** and **2** were recorded with excitation wavelengths of 293 and 316 nm, respectively. Figure 2a exhibits the characteristic transitions of the Tb^{3+} ion at 490, 547, 588, and 623 nm, which are attributed to the $^5D_4 \rightarrow {}^7F_J$ (J = 6, 5, 4, and 3) characteristic transitions, respectively, while Figure 2b displays the characteristic transitions ($^5D_0 \rightarrow {}^7F_J$, where J = 0, 1, 2, 3, and 4) of Eu^{3+} at 578, 592, 613, 650, and 698 nm, respectively. In the emission spectra of **1** and **2**, the characteristic emission of BPDC ligands disappeared. This phenomenon indicated that the transfer of intramolecular energy from the BPDC ligand to Tb^{3+} and Eu^{3+} was much more efficient. As we know, preparing the bimetallic Ln(III)-based MOFs is an efficient strategy for generating multicolored photoluminescence.[1e,f,12a,16] To achieve this goal, we successfully obtained a series of bimetallic Ln(III)-MOFs (Ln = Eu^{3+} and Tb^{3+}) **3**–**6** by solvothermal synthesis. All the bimetallic Ln(III)-MOFs were confirmed by PXRD patterns, and the bimetallic Ln(III)-MOFs matched well with the simulated data and maintained its crystalline integrity (Figure S5). ICP-OES analysis results showed that the Ln(III) composition of the resulting products matched well with the quantity of Ln(III) nitrate used in preparing bimetallic Ln(III)-MOFs. This result indicated that solvothermal synthesis provided a predictable manner for preparing any desired Ln(III) composition in the final product. This foreseeable factor and simple synthesis method was highly appropriate for preparing barcoded materials.

The investigation of luminescence properties revealed the different bimetallic Ln(III) materials could result in discernible and peculiar optic barcoded signals. As shown in Figure 3 and

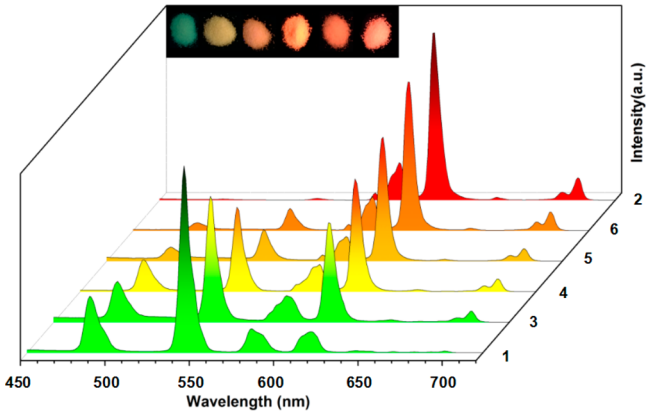

Figure 3. Luminescence emission spectra of **1**–**6** upon excitation at 300 nm and the corresponding images of their luminescence colors under a 254 nm UV lamp.

Figure S6, the emission of bimetallic **3**–**6** showed peculiar characteristic emission peaks from both Eu^{3+} and Tb^{3+} hybrid centers. All the excitation spectra of bimetallic **3**–**6** were broad bands centered at ~300 nm, and the phenomenon occurred because of the simultaneous sensitization by BPDC ligands (Figure S7). This endows the hexanuclear Ln(III) cluster-based MOF with the same excitation band, which was important to the barcoded material application. With an increase in the amount of Eu^{3+} and a proportional decrease in the amount of Tb^{3+} in mixed Ln(III)-MOFs, the red emission intensity was increased while the green emission intensity decreased accordingly. It implied that we could tune the luminescence intensities of Ln(III)-based MOFs via quantitatively controlling the two emitting Ln(III) ions. The mixed hexanuclear Ln(III) cluster-based MOF exhibits a $^5D_4$ (Tb^{3+}) lifetime shorter than that of **1** but a $^5D_0$ (Eu^{3+}) lifetime longer than that of **2**. These phenomena indicated that the energy is transferred from Tb^{3+} to Eu^{3+}. Therefore, in the bimetallic hexanuclear Ln(III) cluster-based MOF, the emission spectra of Eu^{3+} cations can be further sensitized by Tb^{3+} cations within the host framework

DOI: 10.1021/acs.inorgchem.6b02413
Inorg. Chem. 2017, 56, 511–517

(Scheme 2). Theoretically, the efficiency of ET (E) between the donor and the acceptor can be simulated via the luminescence lifetime of the donor.[1e,17,18]

$$E = 1 - \tau_{da}/\tau_{d}$$

Scheme 2. Simplified Diagram of the Ligand-to-Metal Energy Transfer for PL Emission[a] and the Energy Transfer between the Lowest Excited States, $^5D_0$ and $^5D_4$, of the Eu^{3+} and Tb^{3+} Ion Centers

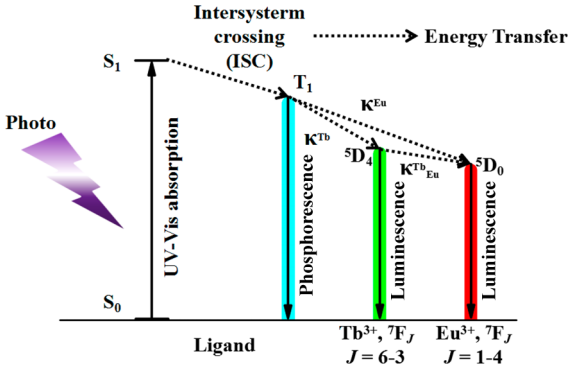

[a] S_0 is the ground state of the ligand; S_1 and T_1 are the singlet state and triplet state of the ligand, respectively.

τ_{da} is the donor's excitation state luminescence lifetime, and τ_{d} is the acceptor's excitation state lifetime. The calculated ET efficiency (E) of the Tb^{3+} cation to Eu^{3+} cation transition in mixed Ln(III)-MOFs composites can exceed 73.3% (Figure 4).

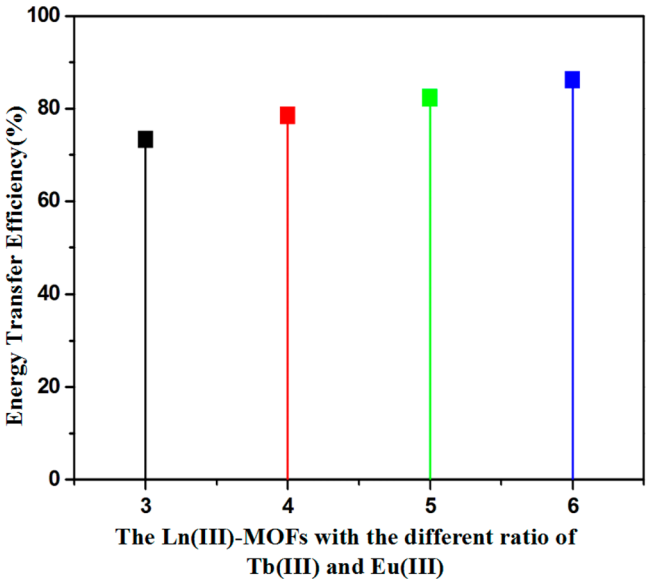

Figure 4. Energy transfer efficiency from Tb^{3+} to Eu^{3+} within Ln(III)-MOFs.

This ET may be prevailingly controlled by the phonon-assisted Förster ET mechanism,[15,17] which represents an essential benefit for the sensitization behavior. With an increase in the Eu^{3+} cation content, the ET efficiency increased gradually. This implies that the regularity of the ET may be caused by regular structural features and permanent porosity of the Ln(III) cluster-based MOF. Furthermore, the relative intensities of compounds **1**−**6** could be reflected as distinct and perceptible color, which is consistent with six different barcodes. As depicted in Figure 5 and Figure S8, the points of emission of **1**, **3**−**6**, and **2** in the CIE diagram were green (X = 0.3187, Y = 0.5598), yellow (X = 0.4058, Y = 0.4810), reddish yellow (X = 0.4612, Y = 0.4531), orange (X = 0.5164, Y = 0.4060), yellowish red (X = 0.5690, Y = 0.3838), and red (X = 0.6282, Y = 0.3485), respectively. The emission colors and the chromaticity coordinates can be systematically tuned with precise correlation to the Eu^{3+}/Tb^{3+} ratios. The excellent linear correlation in color tunability is crucial for application in barcoded materials.[15]

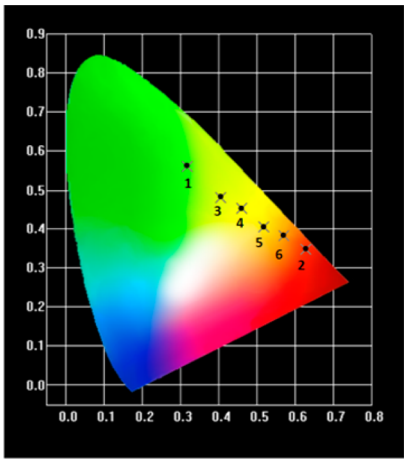

Figure 5. Coordinates of bimetallic hexanuclear Ln(III) cluster-based MOFs **3**−**6** in comparison to those of compounds **1** and **2** upon excitation at 300 nm, showing variation depending on the Tb^{3+}/Eu^{3+} atomic ratio. With a change in the content of Tb^{3+} and Eu^{3+}, the emission color of these materials can be fine-tuned in the RG spectral region.

Organic Dye Selective Removal and Separation. Besides the barcode application, we also explored the potential application of the anionic type hexanuclear Ln(III) cluster-based MOF in organic dye removal.[19] When 20 mg of **1** was soaked in a DMF solution of MB^+ (5 mL, 5×10^{-5} M), it was detected by the UV−vis spectra at room temperature. The Abs peak of MB^+ at 664 nm declined gradually with an increase in soaking time and was almost totally adsorbed (up to 99%) after 24 h, which showed the high-efficiency removal capacity of MB^+ by **1** (Figure 6a).

An excellent adsorbent material needs not only an outstanding adsorption property toward the dyes with a steady nature and easy recyclability but also the eminent capability of selective removal and separation. Thus, three organic dyes, Methyl Orange (MO^-), Sudan I (SD^0), and Crystal Violet (CV^+), were selected as competitive dyes for selective adsorption and separation experiments (Table 1 and Scheme 3). The as-synthesized samples were immersed in the fresh DMF solution containing MO^-, SD^0, or CV^+ under the same condition. The UV−vis absorption intensity of the Abs band of MO^- at 466 nm (Figure S9a), SD^0 at 488 nm (Figure S9b), and CV^+ at 549 nm (Figure S9c) remained unchanged. This good selective adsorption of organic dyes prompted us to study the properties of separation of cationic MB^+ from the mixed MB^+/MO^-, MB^+/SD^0, and MB^+/CV^+ DMF solutions. As displayed in Figure 6b−d, the intensity of the Abs band of MB^+ gradually declined and other characteristic Abs bands remained nearly unchanged, indicating that only the MB^+ in the mixed solutions

DOI: 10.1021/acs.inorgchem.6b02413
Inorg. Chem. 2017, 56, 511−517

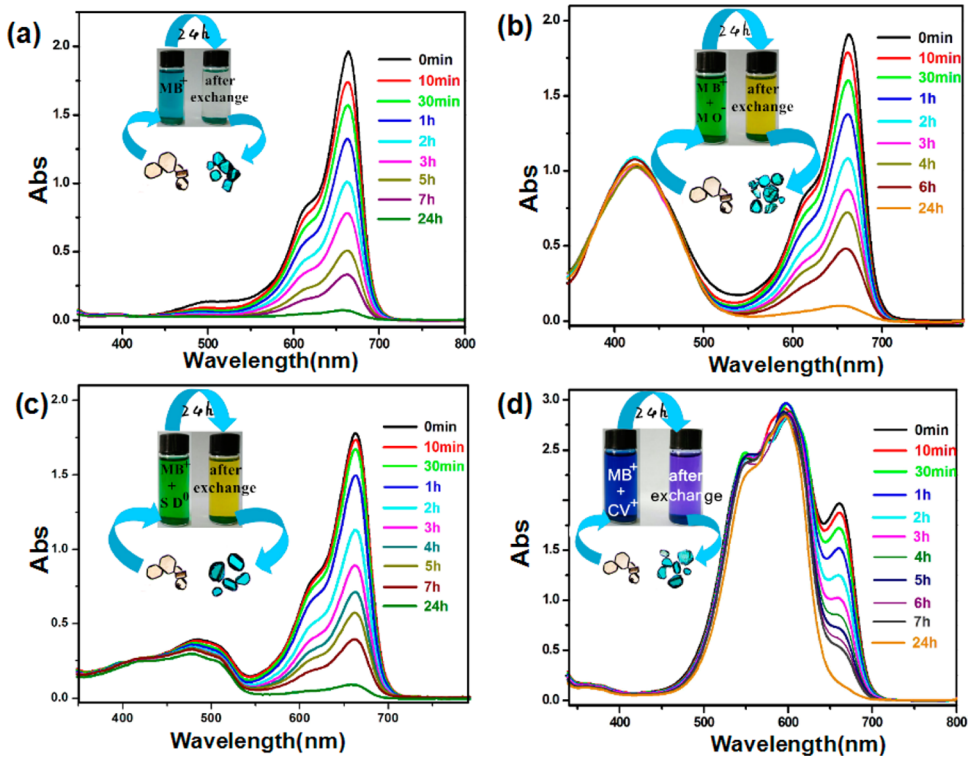

Figure 6. UV−vis spectra of DMF solutions of equimolar dyes in the presence of **1** monitored over time: (a) MB^+, (b) MB^+/MO^-, (c) MB^+/SD^0, and (d) MB^+/CV^+. The photographs show the colors of the dye solutions and the crystalline samples of **1**, before and after ion exchange for 24 h.

Table 1. Molecular Weights and Dimensions of Different Dye Molecules

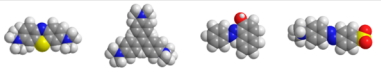

Abbr.	MB^+	CV^+	SD^0	MO^-
M_w	284.40	372.53	248.28	304.33
x(Å)	4.00	4.00	3.68	5.31
y(Å)	7.93	16.32	9.74	7.25
z(Å)	16.34	14.15	13.55	17.39

Scheme 3. Chemical Structures of MB^+, MO^-, SD^0, and CV^+

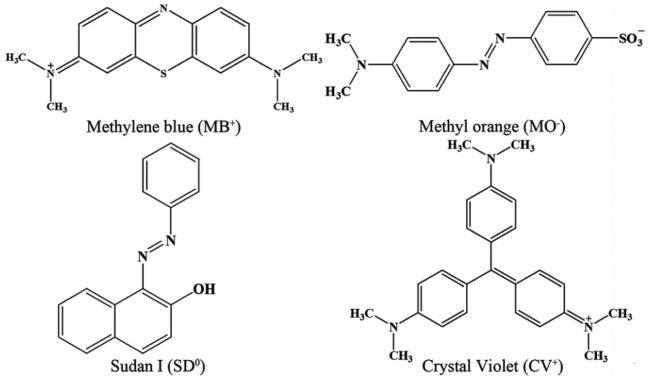

was absorbed by **1**. In a word, other competitive organic dyes had no effect on the MB^+ adsorption capacity of **1**. More exhilaratingly, this selective removal process of MB^+ can even be easily perceived by the naked eye because of the conspicuous change in the color of the mixed solution. Finally, the supernatants were the colors of MO^-, SD^0, and CV^+, and the color of **1** changed to blue (inset of Figure 6b−d). This could be attributed to the anionic framework peculiarity of **1**, and the free countercation DMA^+ reside in the cages could be exchanged with MB^+. However, anionic and neutral dyes could not be absorbed by **1**. Although CV^+ has the same electric charge as MB^+, the larger CV^+ molecules could be excluded from the microspores of **1**. Therefore, anionic type **1** was a good adsorbent for MB^+ removal through the ion-exchange process.

In addition, desorption experiments with MB^+ were also performed and UV−visible spectra detected. The MB^+@**1** sample was soaked into a saturated NaCl/DMF solution (5 mL). As shown in Figure 7 and Figure S10, the Abs peak of the supernatant increased gradually. This phenomenon can be assigned to the entry of Na^+ into the cages of **1** replacing MB^+, which was based on the kinetic equilibrium between different guest species.[19f] For comparison, MB^+@**1** could hardly release MB^+ in a pure DMF solution, proving the replacement of MB^+ with Na^+ really occurs. PXRD of **1** after release confirmed its high stability (Figure S11). This high stability and reversible adsorption feature were crucial to the MB^+ removal application.

CONCLUSIONS

In summary, two new anionic hexanuclear Ln(III) cluster-based MOFs (Ln = Tb and Eu) have been successfully synthesized under solvothermal conditions. In addition, a series of isostructural bimetallic hexanuclear Ln(III) cluster-based MOFs were prepared by changing the ratio of Eu^{3+} to Tb^{3+}. The excellent linear color tunability and dichromatic photoluminescence endow them with the potential for use in barcoded systems in a practical application. In addition, the

DOI: 10.1021/acs.inorgchem.6b02413
Inorg. Chem. 2017, 56, 511−517

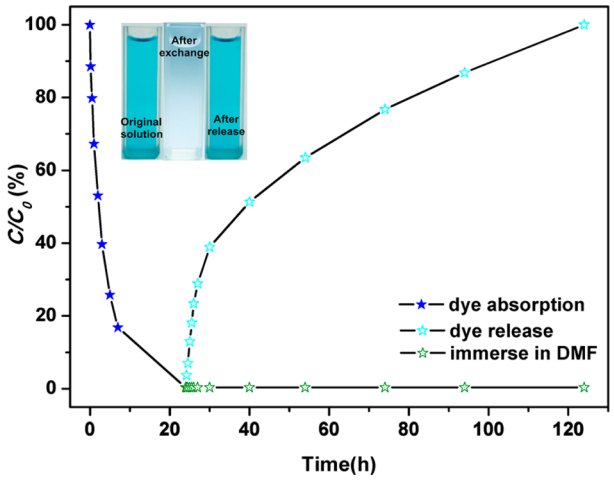

Figure 7. Reversible adsorption and release of MB^+ in a full ion-exchange and release cycle.

anionic hexanuclear Ln(III) cluster-based MOFs exhibit superior uptake capacity toward MB^+ by an ion-exchange process, and the reversible adsorption performance makes **1** suitable for removal of organic dye MB^+. Our ongoing studies are focused on extension of Ln(III) cluster-based MOFs possessing larger porous cages and ionic frameworks with multifunctional properties for use in luminescent materials, adsorption, separation, catalysis, devices, etc.

■ ASSOCIATED CONTENT

Supporting Information

The Supporting Information is available free of charge on the ACS Publications website at DOI: 10.1021/acs.inorgchem.6b02413.

TG curve, PXRD patterns, fluorescence spectra, UV−vis adsorption spectra, decay data, and ICP-OES (PDF)
Crystallographic details (CIF)
checkCIF/PLATON report (PDF)

■ AUTHOR INFORMATION

Corresponding Authors

*E-mail: ceshzb@lnu.edu.cn.
*E-mail: ydq@fjirsm.ac.cn.

ORCID

Zheng-Bo Han: 0000-0001-8635-9783

Author Contributions

M.-L.G. and W.-J.W. contributed equally to this work.

Notes

The authors declare no competing financial interest.

■ ACKNOWLEDGMENTS

This work was financially supported by the National Natural Science Foundation of China (Grants 21671090 and 21271096) and the State Key Laboratory of Rare Earth Resource Utilization (RERU2016002).

■ REFERENCES

(1) (a) Binnemans, K. Lanthanide-Based Luminescent Hybrid Materials. *Chem. Rev.* **2009**, *109*, 4283−4374. (b) Kwok, R. T. K.; Leung, C. W. T.; Lam, J. W. Y.; Tang, B. Z. Biosensing by Luminogens with Aggregation-Induced Emission Characteristics. *Chem. Soc. Rev.* **2015**, *44*, 4228−4238. (c) Meyer, J.; Tappe, F. Photoluminescent Materials for Solid-State Lighting: State of the Art and Future Challenges. *Adv. Opt. Mater.* **2015**, *3*, 424−430. (d) Kamtekar, K. T.; Monkman, A. P.; Bryce, M. R. Recent Advances in White Organic Light-Emitting Materials and Devices (WOLEDs). *Adv. Mater.* **2010**, *22*, 572−582. (e) Guillou, O.; Daiguebonne, C.; Calvez, G.; Bernot, K. A Long Journey in Lanthanide Chemistry: From Fundamental Crystallogenesis Studies to Commercial Anticounterfeiting Taggants. *Acc. Chem. Res.* **2016**, *49*, 844−856. (f) Le Natur, F.; Calvez, G.; Guégan, J. P.; Le Pollès, L.; Trivelli, X.; Bernot, K.; Daiguebonne, C.; Neaime, C.; Costuas, K.; Grasset, F.; Guillou, O. Characterization and Luminescence Properties of Lanthanide-Based Polynuclear Complexes Nanoaggregates. *Inorg. Chem.* **2015**, *54*, 6043−6054.

(2) (a) Bai, G.; Tsang, M. K.; Hao, J. Tuning the Luminescence of Phosphors: Beyond Conventional Chemical Method. *Adv. Opt. Mater.* **2015**, *3*, 431−462. (b) Armelao, L.; Quici, S.; Barigelletti, F.; Accorsi, G.; Bottaro, G.; Cavazzini, M.; Tondelloe, E. Design of luminescent lanthanide complexes: From Molecules to Highly Efficient Photo-Emitting Materials. *Coord. Chem. Rev.* **2010**, *254*, 487−505. (c) Rocha, J.; Carlos, L. D.; Paz, F. A. A.; Ananias, D. Luminescent multifunctional lanthanides-based metal-organic frameworks. *Chem. Soc. Rev.* **2011**, *40*, 926−940.

(3) (a) Du, B. B.; Zhu, Y. X.; Pan, M.; Yue, M. Q.; Hou, Y. J.; Wu, K.; Zhang, L. Y.; Chen, L.; Yin, S. Y.; Fan, Y. N.; Su, C. Y. Direct white-light and a dual-channel barcode module from Pr(III)-MOF crystals. *Chem. Commun.* **2015**, *51*, 12533−12536. (b) Hu, S. H.; Gao, X. Stable Encapsulation of Quantum Dot Barcodes with Silica Shells. *Adv. Funct. Mater.* **2010**, *20*, 3721−3726. (c) Zhang, Y.; Zhang, L.; Deng, R.; Tian, J.; Zong, Y.; Jin, D.; Liu, X. Multicolor Barcoding in a Single Upconversion Crystal. *J. Am. Chem. Soc.* **2014**, *136*, 4893−4896. (d) Santos, A.; Balderrama, V. S.; Alba, M.; Formentín, P.; Ferré-Borrull, J.; Pallarès, J.; Marsal, L. F. Nanoporous Anodic Alumina Barcodes: Toward Smart Optical Biosensors. *Adv. Mater.* **2012**, *24*, 1050−1054.

(4) Yang, Q. Y.; Pan, M.; Wei, S. C.; Li, K.; Du, B. B.; Su, C. Y. Linear Dependence of Photoluminescence in Mixed Ln-MOFs for Color Tunability and Barcode Application. *Inorg. Chem.* **2015**, *54*, 5707−5716.

(5) White, K. A.; Chengelis, D. A.; Gogick, K. A.; Stehman, J.; Rosi, N. L.; Petoud, S. Near-Infrared Luminescent Lanthanide MOF Barcodes. *J. Am. Chem. Soc.* **2009**, *131*, 18069−18071.

(6) (a) Park, D. H.; Hong, Y. K.; Cho, E. H.; Kim, M. S.; Kim, D. C.; Bang, J.; Kim, J.; Joo, J. Light-Emitting Color Barcode Nanowires Using Polymers: Nanoscale Optical Characteristics. *ACS Nano* **2010**, *4*, 5155−5162. (b) Zhang, X.; Xiao, Y.; He, L.; Zhang, Y. Through-Bond Energy Transfer Cassettes for Multicolor Encoding. *J. Org. Chem.* **2014**, *79*, 6315−6320. (c) Krutzik, P. O.; Nolan, G. P. Fluorescent cell barcoding in flow cytometry allows high-throughput drug screening and signaling profiling. *Nat. Methods* **2006**, *3*, 361−368. (d) Wang, L.; Tan, W. Multicolor FRET Silica Nanoparticles by Single Wavelength Excitation. *Nano Lett.* **2006**, *6*, 84−88.

(7) (a) Han, M.; Gao, X.; Su, J. Z.; Nie, S. Quantum-dot-tagged microbeads for multiplexed optical coding of biomolecules. *Nat. Biotechnol.* **2001**, *19*, 631−635. (b) Chen, C.; Zhang, P. F.; Gao, G.; Gao, D.; Yang, Y.; Liu, H.; Wang, Y.; Gong, P.; Cai, L. Near-Infrared-Emitting Two-Dimensional Codes Based on Lattice-Strained Core/(Doped) Shell Quantum Dots with Long Fluorescence Lifetime. *Adv. Mater.* **2014**, *26*, 6313−6317. (c) Zhao, Y. J.; Shum, H. C.; Chen, H. H.; Adams, L. L. A.; Gu, Z.; Weitz, D. A. Microfluidic Generation of Multifunctional Quantum Dot Barcode Particles. *J. Am. Chem. Soc.* **2011**, *133*, 8790−8793. (d) Zhao, Y. J.; Xie, Z. Y.; Gu, H. C.; Jin, L.; Zhao, X.; Wang, B.; Gu, Z. Multifunctional photonic crystal barcodes from microfluidics. *NPG Asia Mater.* **2012**, *4*, e25. (e) Rauf, S.; Glidle, A.; Cooper, J. M. Production of Quantum Dot Barcodes Using Biological Self-Assembly. *Adv. Mater.* **2009**, *21*, 4020−4024. (f) Peng, X. Band Gap and Composition Engineering on a Nanocrystal (BCEN) in Solution. *Acc. Chem. Res.* **2010**, *43*, 1387−1395.

(8) (a) Smith, A. M.; Mohs, A. M.; Nie, S. Tuning the optical and electronic properties of colloidal nanocrystals by lattice strain. *Nat. Nanotechnol.* **2009**, *4*, 56−63. (b) Yang, J.; Dave, S. R.; Gao, X. H.

DOI: 10.1021/acs.inorgchem.6b02413
Inorg. Chem. 2017, 56, 511−517

Quantum Dot Nanobarcodes: Epitaxial Assembly of Nanoparticle-Polymer Complexes in Homogeneous Solution. *J. Am. Chem. Soc.* **2008**, *130*, 5286−5292.
(9) Zhou, Y.; Yan, B. Ratiometric multiplexed barcodes based on luminescent metal-organic framework films. *J. Mater. Chem. C* **2015**, *3*, 8413−8418.
(10) (a) Meng, Q.; Xin, X.; Zhang, L.; Dai, F.; Wang, R.; Sun, D. A multifunctional Eu MOF as a fluorescent pH sensor and exhibiting highly solvent-dependent adsorption and degradation of rhodamine B. *J. Mater. Chem. A* **2015**, *3*, 24016−24021. (b) Wang, X.; Zhang, L.; Yang, J.; Liu, F.; Dai, F.; Wang, R.; Sun, D. Lanthanide metal-organic frameworks containing a novel flexible ligand for luminescence sensing of small organic molecules and selective adsorption. *J. Mater. Chem. A* **2015**, *3*, 12777−12785. (c) Chen, Z.; Sun, Y.; Zhang, L.; Sun, D.; Liu, F.; Meng, Q.; Wang, R.; Sun, D. A tubular europium-organic framework exhibiting selective sensing of Fe^{3+} and Al^{3+} over mixed metal ions. *Chem. Commun.* **2013**, *49*, 11557−11559.
(11) Sheldrick, G. M. *SHELXL-97, Programs for X-ray Crystal Structure Solution*; University of Göttingen: Göttingen, Germany, 1997.
(12) (a) Koh, K.; Wong-Foy, A. G.; Matzger, A. J. A Crystalline Mesoporous Coordination Polymer with High Microporosity. *Angew. Chem., Int. Ed.* **2008**, *47*, 677−680. (b) Hu, S.; He, K. H.; Zeng, M. H.; Zou, H. H.; Jiang, Y. M. Crystalline-State Guest-Exchange and Gas-Adsorption Phenomenon for a "Soft" Supramolecular Porous Framework Stacking by a Rigid Linear Coordination Polymer. *Inorg. Chem.* **2008**, *47*, 5218−5224.
(13) (a) Xue, D. X.; Cairns, A. J.; Belmabkhout, Y.; Wojtas, L.; Liu, Y.; Alkordi, M. H.; Eddaoudi, M. Tunable Rare-Earth fcu-MOFs: A Platform for Systematic Enhancement of CO_2 Adsorption Energetics and Uptake. *J. Am. Chem. Soc.* **2013**, *135*, 7660−7667. (b) Xue, D. X.; Belmabkhout, Y.; Shekhah, O.; Jiang, H.; Adil, K.; Cairns, A. J.; Eddaoudi, M. Tunable Rare Earth fcu-MOF Platform: Access to Adsorption Kinetics Driven Gas/Vapor Separations via Pore Size Contraction. *J. Am. Chem. Soc.* **2015**, *137*, 5034−5040. (c) Luebke, R.; Belmabkhout, Y.; Weseliński, Ł. J.; Cairns, A. J.; Alkordi, M.; Norton, G.; Wojtas, Ł.; Adil, K.; Eddaoudi, M. Versatile rare earth hexanuclear clusters for the design and synthesis of highly-connected ftw-MOFs. *Chem. Sci.* **2015**, *6*, 4095−4102. (d) Alezi, D.; Peedikakkal, A. M. P.; Weseliński, Ł. J.; Guillerm, V.; Belmabkhout, Y.; Cairns, A. J.; Chen, Z.; Wojtas, Ł.; Eddaoudi, M. Quest for Highly Connected Metal-Organic Framework Platforms: Rare-Earth Polynuclear Clusters Versatility Meets Net Topology Needs. *J. Am. Chem. Soc.* **2015**, *137*, 5421−5430.
(14) Spek, A. L. Structure validation in chemical crystallography. *Acta Crystallogr., Sect. D: Biol. Crystallogr.* **2009**, *65*, 148−155.
(15) (a) Cui, Y.; Chen, B.; Qian, G. Lanthanide metal-organic frameworks for luminescent sensing and light-emitting applications. *Coord. Chem. Rev.* **2014**, *273−274*, 76−86. (b) Tang, Q.; Liu, S.; Liu, Y.; Miao, J.; Li, S.; Zhang, L.; Shi, Z.; Zheng, Z. Cation Sensing by a Luminescent Metal-Organic Framework with Multiple Lewis Basic Sites. *Inorg. Chem.* **2013**, *52*, 2799−2801. (c) Zhao, B.; Chen, X. Y.; Cheng, P.; Liao, D. Z.; Yan, S. P.; Jiang, Z. H. Coordination Polymers Containing 1D Channels as Selective Luminescent Probes. *J. Am. Chem. Soc.* **2004**, *126*, 15394−15395.
(16) (a) Zhou, J. M.; Li, H.; Zhang, H.; Li, H.; Shi, W.; Cheng, P. A Bimetallic Lanthanide Metal-Organic Material as a Self-Calibrating Color-Gradient Luminescent Sensor. *Adv. Mater.* **2015**, *27*, 7072−7077. (b) Le Natur, F.; Calvez, G.; Daiguebonne, C.; Guillou, O.; Bernot, K.; Ledoux, J.; Le Pollès, L.; Roiland, C. Coordination Polymers Based on Heterohexanuclear Rare Earth Complexes: Toward Independent Luminescence Brightness and Color Tuning. *Inorg. Chem.* **2013**, *52*, 6720−6730. (c) Freslon, S.; Luo, Y.; Daiguebonne, C.; Calvez, G.; Bernot, K.; Guillou, O. Brightness and Color Tuning in a Series of Lanthanide-Based Coordination Polymers with Benzene-1, 2, 4, 5-tetracarboxylic Acid as a Ligand. *Inorg. Chem.* **2016**, *55*, 794−802.
(17) (a) Zhang, X.; Wang, W.; Hu, Z.; Wang, G.; Uvdal, K. Coordination polymers for energy transfer: Preparations, properties, sensing applications, and perspectives. *Coord. Chem. Rev.* **2015**, *284*, 206−235. (b) Xiao, M.; Selvin, P. R. Quantum Yields of Luminescent Lanthanide Chelates and Far-Red Dyes Measured by Resonance Energy Transfer. *J. Am. Chem. Soc.* **2001**, *123*, 7067−7073.
(18) (a) Auzel, F. Upconversion and Anti-Stokes Processes with f and d Ions in Solids. *Chem. Rev.* **2004**, *104*, 139−174. (b) Liu, Y.; Qian, G.; Wang, Z.; Wang, M. Temperature-dependent luminescent properties of Eu-Tb complexes synthesized in situ in gel glass. *Appl. Phys. Lett.* **2005**, *86*, 071907−07910.
(19) (a) Fei, H.; Rogow, D. L.; Oliver, S. R. J. Reversible Anion Exchange and Catalytic Properties of Two Cationic Metal-Organic Frameworks Based on Cu(I) and Ag(I). *J. Am. Chem. Soc.* **2010**, *132*, 7202−7209. (b) He, Y. C.; Yang, J.; Kan, W. Q.; Zhang, H. M.; Liu, Y. Y.; Ma, J. F. A new microporous anionic metal-organic framework as a platform for highly selective adsorption and separation of organic dyes. *J. Mater. Chem. A* **2015**, *3*, 1675−1681. (c) Oliver, S. R. J. Cationic inorganic materials for anionic pollutant trapping and catalysis. *Chem. Soc. Rev.* **2009**, *38*, 1868−1881. (d) Yang, S.; Lin, X.; Blake, A. J.; Thomas, K. M.; Hubberstey, P.; Champness, N. R.; Schröder, M. Enhancement of H_2 adsorption in Li^+-exchanged co-ordination framework materials. *Chem. Commun.* **2008**, *46*, 6108−6110. (e) Tan, Y.; He, Y.-P.; Zhang, J. ive ion-exchange and self-redox process to load catalytic metal nanoparticles into a MOF with Johnson-type cages. *Chem. Commun.* **2014**, *50*, 6153. (f) Zhao, X.; Bu, X.; Wu, T.; Zheng, S. T.; Wang, L.; Feng, P. Selective anion exchange with nanogated isoreticular positive metal-organic frameworks. *Nat. Commun.* **2013**, *4*, 2344. (g) Liu, L.; Zhang, X. N.; Han, Z. B.; Gao, M. L.; Cao, X. M.; Wang, S. M. An In^{III}-based anionic metal-organic framework: sensitization of lanthanide (III) ions and selective absorption and separation of cationic dyes. *J. Mater. Chem. A* **2015**, *3*, 14157−14164.

DOI: 10.1021/acs.inorgchem.6b02413
Inorg. Chem. 2017, 56, 511−517